Physics of Fluids

Effects of activation energy on the instability of oblique detonation surfaces with a one-step chemistry model

Cite as: Phys. Fluids **30**, 106110 (2018); https://doi.org/10.1063/1.5054063
Submitted: 29 August 2018 • Accepted: 11 October 2018 • Published Online: 30 October 2018

Yining Zhang (张义宁), **Lin Zhou** (周林), **Jishuang Gong** (宫继双), **et al.**

Effects of activation energy on the instability of oblique detonation surfaces with a one-step chemistry model

Yining Zhang (张义宁),[1] Lin Zhou (周林),[1] Jishuang Gong (宫继双),[1] Hoi Dick Ng,[2] and Honghui Teng (滕宏辉)[3]

[1]*State Key Laboratory of Laser Propulsion and Application, Beijing Power Machinery Research Institute, Beijing 100074, China*

[2]*Department of Mechanical, Industrial and Aerospace Engineering, Concordia University, Montreal, Quebec H3G 1M8, Canada*

[3]*School of Aerospace Engineering, Beijing Institute of Technology, Beijing 100081, China*

(Received 29 August 2018; accepted 11 October 2018; published online 30 October 2018)

A numerical study was performed to investigate the detailed effects of activation energy E_a on the oblique detonation wave surface instability. Numerical simulations were performed using an ideal reactive flow model given by the inviscid Euler equations with one-step irreversible Arrhenius reaction kinetics. The numerical results demonstrate two types of unstable structures following the initial smooth surface after detonation initiation. One exhibits by a "saw-tooth" reactive front and the other exhibits by a "keystone" feature. To quantify the destabilization processes, two characteristic length scales, L_1 and L_2, are defined statistically to be the length of the smooth detonation surface before the appearance of instabilities and the length of the unstable surface before the first cellular structure with the onset of right-running transverse waves, respectively. Their dependence on E_a was simulated and analyzed. In general, both lengths decrease with increasing E_a, making the surface more unstable. However, with increasing E_a, the high temperature sensitivity of the mixture causes an abrupt explosion in the initiation region, introducing a high overdriven surface and suppressing the instability. With the balance between the destabilizing effect of E_a and the stabilizing effect of increasing overdrive factor, both L_1 and L_2 are found to approach a near-constant value in the high E_a limit. *Published by AIP Publishing.* https://doi.org/10.1063/1.5054063

I. INTRODUCTION

Air-breathing propulsion systems for hypersonic flight attract more and more attention in recent years.[1,2] Besides the supersonic combustion based on deflagration, the idea of harnessing the power of a standing oblique detonation wave (ODW)[3–6] has long been considered and still attracts great research interest. Early investigations have provided the basic foundation for steady ODWs,[7–9] and later two classical types of initiation structures, i.e., the abrupt[10–12] and smooth[13–15] transition from oblique shock, are observed. The effect of geometry such as the initiation of conical oblique detonation is simulated, illustrating a novel ODW structure.[16] Another geometrical effect includes the finite-wedge inducing the expansion waves, which may quench the detonation or change the wave angle.[17–19] A number of studies have also been carried out addressing the effect of mixture inhomogeneity in the incomplete premixed combustible gas flow,[20–23] illustrating the distorted reaction front and in some cases, the initiation is achieved by a more complex structure. More recently, it was found that decreasing M_0 also results in more involved ODW formation structures, with the induction region observed to end by a set of complicated waves rather than the deflagration wave.[24–28] Furthermore, the transient processes induced by the variation of wedge angle θ were studied recently, illustrating the transition of two different initiation structures.[29]

With regard to an established ODW, numerical investigations have demonstrated that its surface is inherently unstable with fine-scale instability features, similar to the unstable frontal structure of normal cellular detonations in tubes.[30,31] Cellular surfaces were observed in both the experimental[32] and numerical studies.[33] Choi *et al.*[34] performed a detailed numerical study of ODW surface instability, demonstrating the effects of grid resolution and activation energy E_a for the first time. It is thought that the high overdriven degree f_{od} suppresses the formation of cellular surfaces.[35,36] However, our recent study[37] demonstrated that high E_a, i.e., 50 non-dimensionalized by inflow parameters, makes the surface eventually unstable after very long evolution regardless of the high f_{od} degree. A following study[38] has illustrated two types of cellular structures, one is featured by LRTW (left-running transverse waves) and the other is featured by additional RRTW (right-running transverse waves). Based on those processes, two characteristic lengths dependent on E_a and θ are proposed to quantify the destabilized processes. Another recent study[39] demonstrates that the ODW surface instability is associated with the initiation region, from where the disturbance origins.

Although ODW surface instability has been studied widely in a number of studies, those provide mainly isolated results and lack an underlying connection. Often different inflow parameters and chemistry models are employed. As the simplest model, one-step irreversible Arrhenius reaction

kinetics could provide fundamental results, which are crucial to simplifying results from various models and interpret the underlying physics, e.g., recent studies on detonation propagation.[40,41] A previous ODW study[38] based on this chemistry model has revealed the characteristic lengths dependent on E_a and θ, but E_a is limited in a narrow range around 30. Equivalent to normal detonations,[30,31,40,41] E_a is vital in the detonation dynamics, so in this study its effects on surface instability are studied further with a wider range from 30 to 50. By simulating the ODW structure and analyzing the destabilization evolution, effects of activation energy on the oblique detonation surface instability are discussed in detail.

II. PHYSICAL MODEL AND COMPUTATIONAL METHOD

A schematic of the wedge-induced oblique detonation is shown in Fig. 1. The combustible supersonic inflow with Mach number M_0 reflects on the two-dimensional wedge with angle θ, and high temperature behind the oblique shock wave (OSW) may trigger exothermic chemical reactions and lead to the onset of an oblique detonation wave. For the present numerical study, the computational domain is shown in the region bounded by the dashed line, whose coordinates are aligned with the wedge surface, following essentially our previous studies, e.g., Refs. 26–29. Previous results[13,42] demonstrate that the viscosity and boundary layer have little effects on the overall ODW structure, different from the supersonic combustion,[43–48] and most of the research carried out before is based on the inviscid assumption. The non-dimensional governing equations with a single-step, irreversible chemical reaction are of the form

$$\frac{\partial U}{\partial t}+\frac{\partial E}{\partial x}+\frac{\partial F}{\partial y}+S=0, \tag{1}$$

$$U=\begin{bmatrix}\rho\\ \rho u\\ \rho v\\ \rho e\\ \rho\lambda\end{bmatrix},\ E=\begin{bmatrix}\rho u\\ \rho u^2+p\\ \rho uv\\ \rho u(e+p)\\ \rho u\lambda\end{bmatrix},\ F=\begin{bmatrix}\rho v\\ \rho uv\\ \rho v^2+p\\ \rho v(e+p)\\ \rho v\lambda\end{bmatrix},\ S=\begin{bmatrix}0\\ 0\\ 0\\ 0\\ \dot{\omega}\end{bmatrix}, \tag{2}$$

with

$$e=\frac{p}{(\gamma-1)\rho}+\frac{1}{2}\left(u^2+v^2\right)-\lambda Q, \tag{3}$$

$$p=\rho T, \tag{4}$$

$$\omega=-k\rho(1-\lambda)\exp(-E_a/T). \tag{5}$$

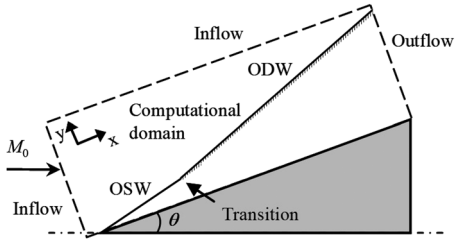

FIG. 1. A schematic of an oblique detonation wave induced by the wedge in the combustible gas mixtures.

TABLE I. Pre-exponential factor used in different cases.

E_a	k
30	80.2
35	182.6
40	423.9
45	1002.4
50	2411.4

All the flow variables have been made dimensionless by reference to the uniform unburned state ahead of the detonation front,

$$\rho=\frac{\tilde{\rho}}{\tilde{\rho}_0},\ p=\frac{\tilde{p}}{\tilde{p}_0},\ T=\frac{\tilde{T}}{\tilde{T}_0},\ u=\frac{\tilde{u}}{\sqrt{\tilde{R}\tilde{T}_0}},\ Q=\frac{\tilde{Q}}{\tilde{R}\tilde{T}_0},\ E_a=\frac{\tilde{E}_a}{\tilde{R}\tilde{T}_0}. \tag{6}$$

For the chemical reaction, λ is the reaction progress variable which varies between 0 (for unburned reactant) and 1 (for product). The reaction is controlled by E_a and the pre-exponential factor k, which is chosen to define the spatial and temporal scales, so the half reaction zone length is unit. E_a and the corresponding k are shown in Table I.

The governing equations are discretized on Cartesian uniform grids and solved numerically using the MUSCL-Hancock scheme with Strang's splitting. The MUSCL-Hancock scheme is formally a second-order extension to Godunov's first order upwind method by constructing the Riemann problem on the inter-cell boundary.[49] The scheme is made total variation diminishing (TVD) with the use of slope limiter MINBEE, and the Harten-Lax-van Leer-Contact (HLLC) approximate solver is used for the Riemann problem.

In this study, we use the dimensionless parameters $Q=50$ and $\gamma=1.2$. These are used traditionally in numerical simulations as canonical values to investigate detonation wave phenomena in general, only different activation energies are considered here. Initially the whole flow field has uniform density, velocity, and pressure. Both the density and pressure are unity as the unburned state, and the velocity is calculated and projected according to M_0 and θ. Inflow conditions are fixed at the free-stream values in both the left and upper boundaries of the domain. Outflow conditions extrapolated from the interior are implemented on the right and lower boundaries before the wedge. Slip boundary conditions are used on the wedge surface, which starts from $x=0.5$ on the lower boundary. In all simulations of this study, M_0 and θ are fixed at 12.5 and 26°, respectively. The default numerical resolution is 32 points per half reaction length which will be verified in the subsequent resolution study.

III. RESULTS AND DISCUSSION

A. Flow structures and resolution study

The flow fields displayed by pressure and temperature for $E_a=30$ and 35 are shown in Fig. 2. In this study, the computational domains are adjusted case by case to provide the best results for illustration. It is observed that the OSW-ODW transition occurs around $x=20$ in both cases, and the smooth surface of ODW appears after the initiation.

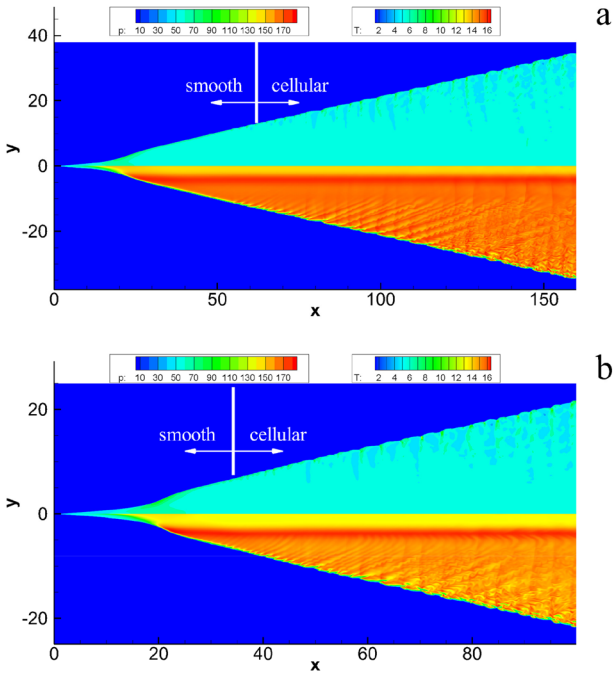

FIG. 2. Pressure (upper) and temperature (lower) with $E_a = 30$ (a) and 35 (b).

However, the ODW surface becomes cellular due to the formation of triple points. Effects of E_a can be observed from the destabilization process qualitatively, i.e., a long smooth surface shown in Fig. 2(a), while a shorter one in Fig. 2(b) for higher E_a. This indicates that increasing E_a makes the surface more unstable, which is similar to the instability of normal detonations.[30,31]

To investigate the onset of surface instability, local structures at a certain instant shown by temperature and half reaction surface are given in Fig. 3. The initial destabilization process is achieved by the gradual formation of "saw-tooth" type reactive front, as shown in Fig. 3(a). This type of cellular structure derives from the formation of LRTWs, although they are convected downstream due to high M_0. It is observed that the cell width becomes large near the right boundary of Fig. 3(a). This provides the circumstances of the successive destabilization process, and the second type of cellular structures is featured by additional RRTWs. As shown in Fig. 3(b), the "keystone" type reactive front appears, which can be viewed as the distorted cellular structure of normal detonations in oblique supersonic inflow. The Mach numbers near the local structures are plotted and marked in Fig. 4. Given inflow Mach number $M_0 = 12.5$, the post-detonation Mach number decreases to below 3.0, but the whole flow field remains supersonic. Because of the high Mach number, all triple points on the detonation surface are convected downstream, even for LRTWs which face upstream, as indicated in Fig. 4(a). The rapid Mach number variation appears near the surface, and the second cellular structure induces more complicated Mach number distribution as shown in Fig. 4(b). Generally, these results are similar to previous studies,[34,38] but higher E_a values are further investigated in this study.

To clarify whether the grid scale affects the numerical results, resolution studies are performed by using finer grids. The results from Figs. 2–4 are based on the resolution of 32 grids per half reaction length, and additional simulations are performed using the resolution of 64 grids per half reaction length. Figure 5 compares the results with $E_a = 35$ and 50 based on two different resolutions, demonstrating that the results are almost independent on the resolution. Both the oblique shock/detonation wave angles and the initiation positions agree with each other. Furthermore, the formation positions of two types of cellular structures, which are very sensitive to the numerical resolution, are almost the same. Pressure and temperature curves along the line $y = 4$ in the case of $E_a = 30$ and $y = 2$ in the case of $E_a = 50$, corresponding the newly formed smooth surfaces, are plotted in Fig. 6. It is observed that the difference is negligible except the downstream region, which is associated with the instability of the slip line nearby. To further verify the resolution effects, the positions of the half reaction zone along the line paralleled with the x-axis are recorded. On the smooth surface, it is fixed at a certain position but varies when the surface becomes unstable. Figure 7 shows the pressure oscillation of the half reaction zone along different lines, $y = 5$ and 8, with different resolutions. Along the line $y = 5$, the weakly unstable surface has a small amplitude oscillation, which becomes large along the line $y = 8$. Generally, the

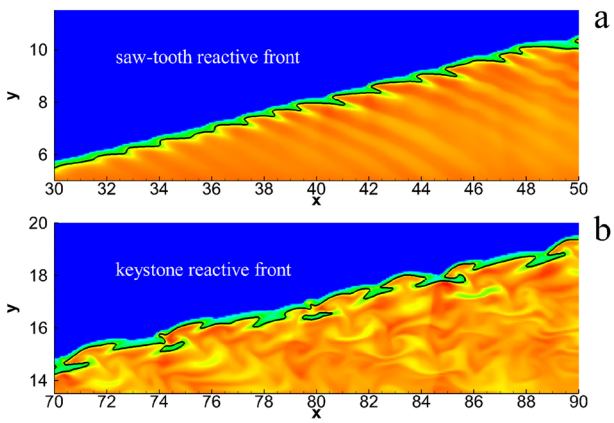

FIG. 3. Local fine structures shown by the temperature field and half reaction location (black line) on the surface with $E_a = 35$.

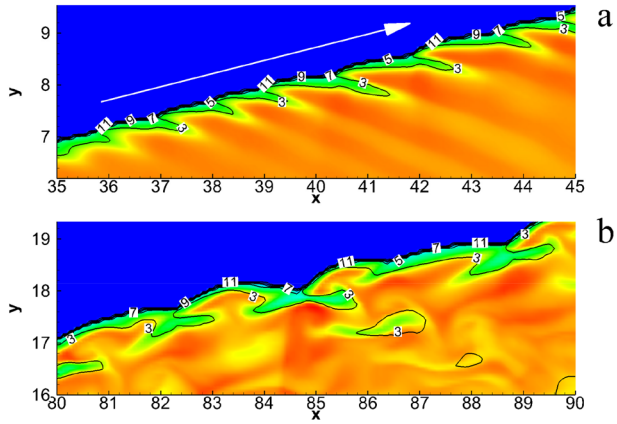

FIG. 4. Local fine structures by the temperature field and Mach number (black line) on the surface $E_a = 35$.

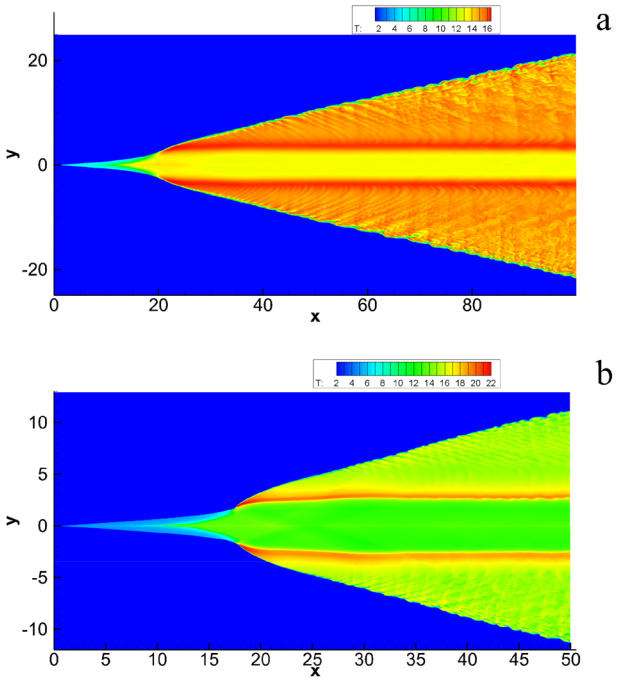

FIG. 5. Temperature with 32 (upper) and 64 (lower) grids per half reaction length with $E_a = 35$ (a) and 50 (b).

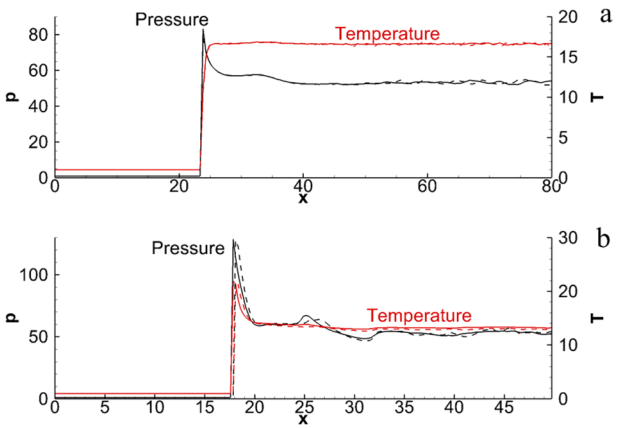

FIG. 6. Pressure and temperature with 32 (solid) and 64 (dashed) grids per half reaction length on the line (a) $y = 4$, $E_a = 35$ and (b) $y = 2$, $E_a = 50$.

amplitude is independent of grid resolution, although totally overlapping is not feasible due to the randomness of the surface instability. Overall, all these results demonstrate that the grid resolution of 32 grids per half reaction length is enough to get convergence of the numerical results investigated in this study, so it is used in the following simulations.

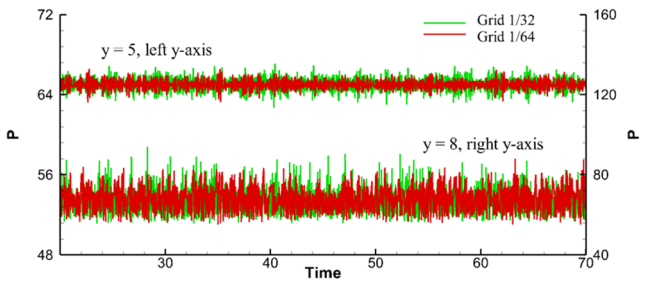

FIG. 7. Pressure oscillation with 32 (upper) and 64 (lower) grids along the lines $y = 5$ and 8 with $E_a = 35$.

To elucidate the effects of activation energy on the ODW dynamics, the simulation results with higher E_a, i.e., 40 and 50, are shown in Fig. 8. It is observed that increasing E_a makes the surface more unstable (i.e., earlier onset of cellular instability), so the length of the smooth surface decreases. Meanwhile, there are obvious changes of ODW structures observed in Fig. 8. First, the OSW-ODW transition is achieved by a curved shock in the case of low E_a, e.g., 30 and 40, while a multi-wave point can be observed as the transition becomes the abrupt one in the case of $E_a = 50$ in Fig. 8(b). This abrupt transition is coupled with a slip line, whose front tip bends toward the wedge. Furthermore, the slip line becomes unstable so the vortex formation is observed downstream, demonstrating high E_a promotes the Kelvin-Helmholtz instability in the detonation product.

The ODW flow fields are transient with the dynamic cellular surface, but above figures only show a snapshot of flow field at a certain instant. To examine the general characteristics of ODW dynamics, numerical smoked foil records using maximum pressure trace are also generated during the computation. Before the simulation, a long region where ODW will propagate through is prescribed with inflow pressure. During the simulation, when the ODW sweeps the region, the saved pressure value will be compared with the pressure around the ODW and the larger one will be recorded. For the detonation, the maximum pressure usually appears near the triple points, and hence, this method will generate the triple point traces to display the cellular surface, which has a similar effect with the experimental smoked foil. Figure 9 shows the numerical foil records with $E_a = 30$, 40, and 50. The initiation is illustrated by a transverse high-pressure region, and as described above, the ODW surfaces are composed of three sections after initiation.

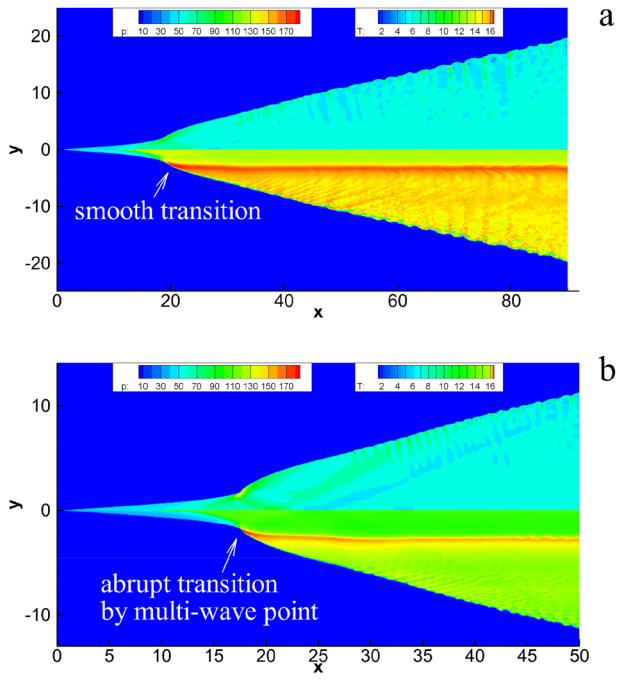

FIG. 8. Pressure (upper) and temperature (lower) with $E_a = 40$ (a) and 50 (b).

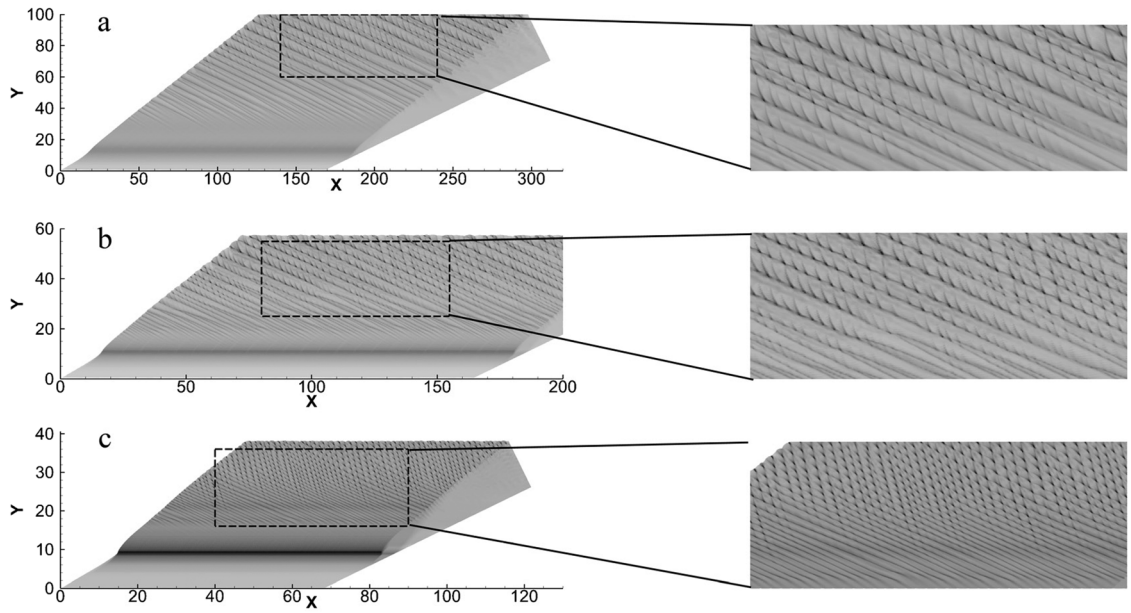

FIG. 9. Numerical smoked foil records with E_a = 30 (a), 40 (b), and 50 (c).

The first sections are smooth that can locate around y = 20–30 in Fig. 9(a), y = 15–20 in Fig. 9(b), and y = 10–15 in Fig. 9(c). Above the smooth section, the first fine structure changes the surface to be unstable, which is featured by LRTWs and hence, the trajectory of one group of triple points. The formation of the second fine structure results in the third section, in which RRTWs are observed clearly, as shown in the zoomed-in pictures. By comparing different frames in Fig. 9, it is observed that the formations of both LRTW and RRTW depend on E_a significantly. Further analysis is necessary to characterize the flow field and quantify the instability.

To study the quantitative difference of numerical cells, Fig. 10 shows the pressure curves along x = 60 of numerical smoked foil records from E_a = 30 and 50 in Fig. 9. With the same M_0, the pressure is increased by the OSW to the same value regardless of different E_a. However, the subsequent heat release process depends on the reaction sensitivity governed by E_a. In the case of high E_a, i.e., 50, a severe explosion at the initiation point is generated. The pressure peak of the initiation region can reach as high as about 150, while the peak is about 80 in the case of low E_a, i.e., 30. Furthermore, high E_a induces the rapid destabilization process, which is illustrated by the multi-peak pressure on the E_a = 50 curve.

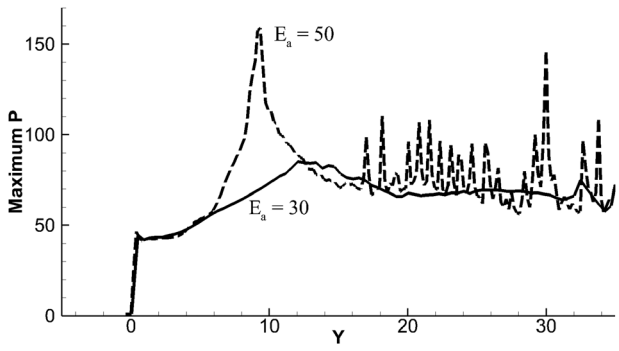

FIG. 10. Pressure along x = 60 of numerical smoked foil in Fig. 9.

It is worth mentioning that the equilibrium pressure in the far field should be independent of E_a if the ODW surface remains smooth. However, E_a changes the initiation region and the following destabilization process, so different ODW structures are observed.

B. Analysis of the characteristic lengths

To provide a quantitative measurement of the surface instability, a statistic analysis method has been proposed,[38] which is inspired by the work of Sharpe and Radulescu on irregular detonation cells.[50] Two key positions, KP1 and KP2, have been defined, in which KP1 corresponds to the location where LRTW first emerges, and KP2 corresponds to the one where RRTW emerges. KP1 and KP2 are used to define the characteristic length scales L_1 and L_2, which stand for the smooth surface length and the first cellular surface length, respectively. L_1 starts at the detonation initiation point and terminates at KP1, while L_2 starts at KP1 and ends at KP2, see Fig. 11(a). The values of KP1 and KP2 are not at certain instant but calculated based on the long-time computation after the oblique detonation is formed. The instantaneous locations of these key points are saved every several steps, and if the total steps are large enough, significant amounts of instantaneous key points can be recorded. The probability of KP1 and KP2 on certain positions can then be calculated through post-processing, so independent on the non-stationary flow. This method eliminates the uncertainty induced by the instability, and it is indeed found that the probability profiles are almost invariable if the obtained number of instantaneous key points is large enough.

The probability distributions of KP1 and KP2 and their cumulative values are shown in Figs. 11(b) and 11(c). In the case of E_a = 40, KP1 moves in a narrow range around 30 and KP2 moves in a wide range around 50–90, as shown in Fig. 11(b). Other cases follow similar KP1 and KP2 distributions. Figure 11(c) shows the cumulative probability

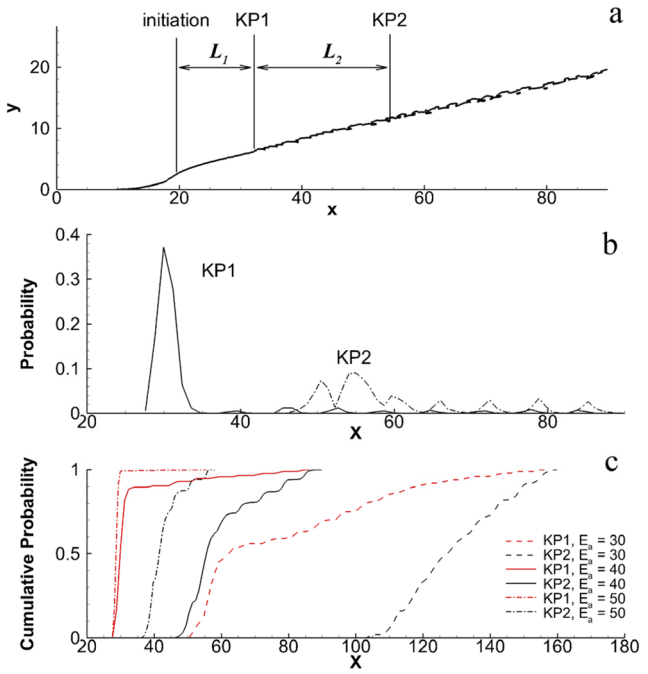

FIG. 11. (a) Definition of characteristic length scales, L_1 and L_2; (b) probability distributions of KP1 and KP2 with $E_a = 40$; (c) cumulative Probability distributions with $E_a = 30$, 40, and 50.

distributions of the cases with E_a = 30, 40, and 50. It is observed that both KP1 and KP2 locate downstream in the case of E_a = 30 and move upstream when E_a increases. Furthermore, high E_a compresses the length of the region where KP1 and KP2 may appear. Comparing all six plots in Fig. 11(c), there is always a rapid increase of the KP1 curve in each case, but not on the KP2 curve. This suggests that the second destabilization process is more complicated and harder to be predicted, similar to the observed phenomena in our previous study.[38]

To quantify the destabilization characteristics, we use 50% probability to indicate the position of KP1 and KP2, so the quantities of L_1 and L_2 can be determined. The dependence of these lengths on E_a is shown in Fig. 12. When E_a increases from 30 to 50, L_1 decreases first and approaches almost to a constant when E_a is above 35. On the other hand, L_2 decreases monotonically from 30 to 50, and the slow decreasing rate observed at the final stage. It is observed that L_1 and L_2 are almost the same in the case of E_a = 50.

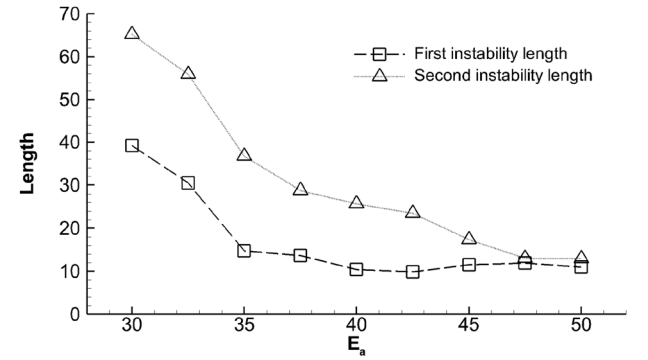

FIG. 12. Two instability lengths as a function of E_a.

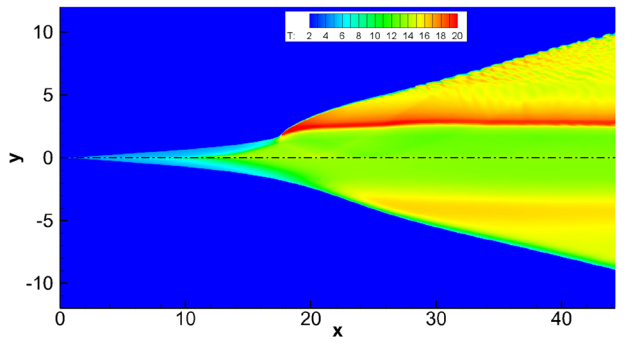

FIG. 13. Temperature of the initiation region with E_a = 50 (upper) and 30 (lower).

Increasing E_a makes the surface more susceptible to instability, so both L_1 and L_2 decrease. Although a very narrow E_a range, from 27 to 33, is employed, a similar trend has been observed in our previous study.[38] However, the present work demonstrates that the dependence of these characteristic lengths on E_a with a wider range has a peculiar behavior. Especially when E_a increases from 35 to 40, the near-constant L_1 appears and its mechanism needs to be clarified. When analyzing the numerical foil records in Fig. 10, the pressure peak in the case of E_a = 50 is about twice of that in the case of E_a = 30, suggesting that the difference in the initiation may be responsible to the following destabilization process. Figure 13 compares the temperature fields of the initiation region with E_a = 50 and 30. Notably, the OSW-ODW transitions are different, the smooth one for low E_a and abrupt one for high E_a, resulting in different local structures. In the case of E_a = 50, there is a quick increase of oblique detonation angle β just after initiation. Conversely, the oblique detonation angle increase is moderate in the case of E_a = 30. As studied before,[37] high oblique detonation angle induces high overdriven degree f_{od}, defined by $(M_0 \sin\beta/M_{CJ})^2$, which suppresses the formation of triple points.

To examine the effect of f_{od} quantitatively, the local overdriven degrees of smooth ODW surfaces for the cases E_a = 30, 40, and 50 are shown in Fig. 14. It is observed that the highest f_{od} in the case of E_a = 30 is below 1.8, and f_{od} decreases gradually when surface extends downstream. Increasing E_a not only moves the initiation points upstream but also raises its highest f_{od}. The quantities of initiation position and f_{od} dependent on E_a are listed in Table II. It shows that the average f_{od} increases when E_a increases, and all of them are higher

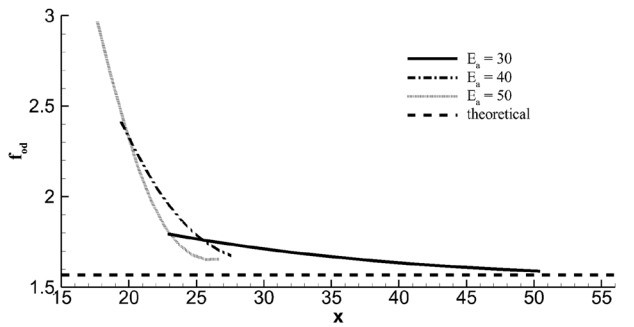

FIG. 14. Overdriven degree of smooth surfaces with E_a = 30, 40, and 50.

TABLE II. Initiation position and f_{od} in different cases.

E_a	Initial position	f_{od}
30	22.86	1.67
35	20.82	1.83
40	19.44	1.96
45	18.51	2.00
50	17.67	2.04

than 1.57 (the theoretical f_{od}). The theoretical value is predicted by oblique detonation relations, only appears when the oblique detonation angle reaches its equilibrium state without the appearance of unstable surface. These results demonstrate that the destabilization process occurs in a non-equilibrium oblique detonation surface, in which high E_a plays double roles on the instability. One role is accelerating the instability, which has been pointed out before. The other role is introducing the high f_{od} as a consequence of an abrupt explosion due to increasing mixture reaction sensitivity with high E_a, so suppressing the instability. Due to these competing effects, the L_1 curve shows a near-constant regime when E_a increases.

It may be useful to compare this work with two recent studies concerning the destabilized process.[16,39] ODWs behind the 2-D shock are simulated based on Euler equations with a two-step induction-reaction kinetic model,[39] and a new instability mechanism derives from the perturbation of the initiation region is proposed. Although only the first destabilized process is concerned there, the conclusion, i.e., enhancing the instability of detonation will decrease the length of smooth surface, is the same as this study excepting the detonation instability is controlled by different parameters. However, with the same one-step irreversible heat release model but conical shock, the formation of unstable surfaces in Ref. 16 appears different from this study. In a limited computational domain with the same E_a, cellular surfaces are observed in the cases of high θ, but not the cases of low θ. High θ induces the high f_{od}, which should be difficult to destabilize. However, the effect of conical flow, also known as Taylor-Maccoll flow, introduces a novel structure concerning the uncoupling of shock and heat release. Then the slow decaying of f_{od}, as shown in Fig. 14, is interrupted and only occurs after the second initiation point. These results demonstrate that the destabilized process of ODW should be studied after a successful initiation, so a continuous decay of overdriven degree is possible. In addition, these comparisons indicate that the phenomenon is controlled by different effects and modeling details, hence each single parameter, such as the activation energy E_a in this study, should be explored fully to reveal all the possible observations and associated processes, even within an idealized model framework to build upon.

After the first destabilized process, the surface evolution and formation of "key-stone" reactive front occurs on the cellular surface, which is hard to perform the above analysis. However, the slow decreasing rate of L_2 is observed as shown in Fig. 12, demonstrating a similar trend of L_1 from E_a 30 to 40. Theoretically, the high f_{od} should also influence the second destabilized process because both of them concern the formation of triple points essentially. The effects of high f_{od} become intense when L_1 decreases, so the second process occurs upstream. Therefore, in the high-activation-energy limit, both L_1 and L_2 appear to converge and approach to a near constant value.

Based on the Euler equations with a one-step irreversible Arrhenius chemistry model, ODW structures are simulated and effects of E_a on the destabilized processes are clarified. More fruitful phenomena are observed based on the advanced model, such as the detailed chemistry or two-step chain-branching models. This study is actually a fundamental work which should be fully explored before. There are several controlling parameters in the advanced model, and analyzing those results is not a trivial study. This study provides the fundamental knowledge of the simplest unstable ODWs, which ignores several effects and the incident Mach number is not chosen to simulate certain flight conditions. In the future, besides the advanced realistic chemistry model, several effects should be considered to approach the realistic flow. Especially the turbulence-like reactive front appears, the inclusion of compressible turbulence will be an important task. However, simulating turbulence and its effects behind a self-sustained detonation wave at high Reynolds numbers remains computationally challenging, if not forbidden. There is still a research gap and much to learn even using an ideal inviscid detonation model. Nevertheless, several studies[43–48] on the coupling of turbulence and heat release have performed, which is crucial to achieve air-breathing supersonic combustion.[2] These enlightening results deserve more attention and should complement in the further ODW studies.

IV. CONCLUSION

Oblique detonation waves (ODWs) are simulated using the inviscid Euler equations with a one-step irreversible Arrhenius chemistry model. This numerical study investigates in detail the effects of activation energy E_a on the ODW surface instability behavior, particularly focusing on the initial ODW structure evolution and analyzing the destabilization processes.

The numerical results demonstrate that the smooth surface appears after initiation and then destabilizes to generate the front with local fine structures. Two types of structures are observed, one is featured by "saw-tooth" reactive front, and the other is featured by "keystone" reactive front evolved from the first one. To quantify the feature of unstable surfaces, we define the first and second instability lengths, L_1 and L_2, by the lengths of smooth surface and "saw-tooth" reactive front, respectively. When E_a increases from 30 to 50, L_2 decreases monotonically, while L_1 decreases initially and approaches to almost a constant. To explain the variation of these two characteristic lengths, the initiation structures and corresponding f_{od} values near the initiation region are plotted. Generally, high E_a makes the surface unstable and promotes the appearance of cellular instabilities, so increasing E_a destabilizes the surface, i.e., decreasing L_1 and L_2. On the other side, the first destabilization process occurs close to the initiation region where the high temperature reaction sensitivity (high E_a) causes an abrupt explosion introducing high f_{od}. The high

overdriven effect suppresses the instability, resulting in a larger destabilized length. Due to the competing effects, the L_1 curve shows a near-constant regime and the slow decreasing rate of L_2 is observed when E_a increases.

ACKNOWLEDGMENTS

The research is supported by the National Natural Science Foundation of China NSFC (Nos. 11822202 and 91641130) and the Natural Sciences and Engineering Research Council of Canada NSERC (No. RGPIN-2017-06698).

[1] E. T. Curran, W. H. Heiser, and D. T. Pratt, "Fluid phenomena in scramjet combustion systems," Annu. Rev. Fluid. Mech. **28**, 323–360 (1996).
[2] J. Urzay, "Supersonic combustion in air-breathing propulsion systems for hypersonic flight," Annu. Rev. Fluid. Mech. **50**, 593–627 (2018).
[3] J. L. Cambier, H. Adelman, and G. P. Menees, "Numerical simulations of an oblique detonation wave engine," J. Propul. Power **6**, 315 (1990).
[4] D. T. Pratt, J. W. Humphrey, and D. E. Glenn, "Morphology of standing oblique detonation waves," J. Propul. Power **7**, 837 (1991).
[5] G. P. Menees, H. G. Adelman, J. L. Cambier, and J. V. Bowles, "Wave combustors for trans-atmospheric vehicles," J. Propul. Power **8**, 709 (1992).
[6] F. K. Lu, H. Fan, and D. R. Wilson, "Detonation waves induced by a confined wedge," Aerosp. Sci. Technol. **10**, 679 (2006).
[7] R. A. Gross, "Oblique detonation waves," AIAA J. **1**, 1225 (1963).
[8] S. A. Ashford and G. Emanuel, "Wave angle for oblique detonation waves," Shock Waves **3**, 327 (1994).
[9] G. Emanuel and D. G. Tuckness, "Steady, oblique, detonation waves," Shock Waves **13**, 445 (2004).
[10] C. Li, K. Kailasanath, and E. S. Oran, "Detonation structures behind oblique shocks," Phys. Fluids **6**, 1600–1611 (1994).
[11] J. P. Sislian, R. Dudebout, J. Schumacher, M. Islam, and R. Oppitz, "Inviscid propulsive characteristics of hypersonic shcramjets," AIAA Paper No. 96-4535 (1996).
[12] C. Viguier, L. F. Figueira Da Silva, D. Desbordes, and B. Deshaies, "Onset of oblique detonation waves: Comparison between experimental and numerical results for hydrogen-air mixture," Symp. (Int.) Combust. **26**, 3023 (1996).
[13] L. F. Figueira Da Silva and B. Deshaies, "Stabilization of an oblique detonation wave by a wedge: A parametric numerical study," Combust. Flame **121**, 152 (2000).
[14] H. H. Teng and Z. L. Jiang, "On the transition pattern of the oblique detonation structure," J. Fluid Mech. **713**, 659 (2012).
[15] T. Wang, Y. Zhang, H. Teng, Z. Jiang, and H. D. Ng, "Numerical study of oblique detonation wave initiation in a stoichiometric hydrogen-air mixture," Phys. Fluids **27**, 096101 (2015).
[16] P. Yang, H. D. Ng, H. Teng, and Z. Jiang, "Initiation structure of oblique detonation waves behind conical shocks," Phys. Fluids **29**, 086104 (2017).
[17] S. Bhattrai and H. Tang, "Formation of near-Chapman–Jouguet oblique detonation wave over a dual-angle ramp," Aerosp. Sci. Technol. **63**, 1 (2017).
[18] Y. Liu, X. D. Han, S. B. Yao, and J. P. Wang, "A numerical investigation of the prompt oblique detonation wave sustained by a finite-length wedge," Shock Waves **26**, 729 (2016).
[19] Y. Fang, Z. Hu, and H. Teng, "Numerical investigation of oblique detonations induced by a finite wedge in a stoichiometric hydrogen-air mixture," Fuel **234**, 502 (2018).
[20] K. Iwata, S. Nakaya, and M. Tsue, "Wedge-stabilized oblique detonation in an inhomogeneous hydrogen–air mixture," Proc. Combust. Inst. **36**, 2761 (2017).
[21] Y. Zhang, J. Gong, and T. Wang, "Numerical study on initiation of oblique detonations in hydrogen–air mixtures with various equivalence ratios," Aerosp. Sci. Technol. **49**, 130 (2016).
[22] G. Fusina, J. P. Sislian, and B. Parent, "Formation and stability of near Chapman-Jouguet standing oblique detonation waves," AIAA J. **43**, 1591 (2005).
[23] Y. Fang, Z. Hu, H. Teng, Z. Jiang, and H. D. Ng, "Numerical study of inflow equivalence ratio inhomogeneity on oblique detonation formation in hydrogen–air mixtures," Aerosp. Sci. Technol. **71**, 256 (2017).
[24] Y. Liu, D. Wu, S. B. Yao, and J. P. Wang, "Analytical and numerical investigations of wedge-induced oblique detonation waves at low inflow Mach number," Combust. Sci. Technol. **187**, 843 (2015).
[25] J. Y. Choi, E. J. R. Shin, and I. S. Jeung, "Unstable combustion induced by oblique shock waves at the non-attaching condition of the oblique detonation wave," Proc. Combust. Inst. **32**, 2387 (2009).
[26] H. Teng, Y. Zhang, and Z. Jiang, "Numerical investigation on the induction zone structure of the oblique detonation waves," Comput. Fluids **95**, 127 (2014).
[27] H. Teng, H. D. Ng, and Z. Jiang, "Initiation characteristics of wedge-induced oblique detonation waves in a stoichiometric hydrogen-air mixture," Proc. Combust. Inst. **36**, 2735 (2017).
[28] P. Yang, H. Teng, Z. Jiang, and H. D. Ng, "Effects of inflow Mach number on oblique detonation initiation with a two-step induction-reaction kinetic model," Combust. Flame **193**, 246 (2018).
[29] Y. Zhang, P. Yang, H. Teng, H. D. Ng, and C. Wen, "Transition between different initiation structures of wedge-induced oblique detonations," AIAA J. **56**, 4016 (2018).
[30] V. N. Gamezo, D. Desbordes, and E. S. Oran, "Two-dimensional reactive flow dynamics in cellular detonation waves," Shock Waves **9**, 11 (1999).
[31] V. N. Gamezo, D. Desbordes, and E. S. Oran, "Formation and evolution of two-dimensional cellular detonations," Combust. Flame **116**, 154 (1999).
[32] C. Viguier, A. Gourara, and D. Desbordes, "Three-dimensional structure of stabilization of oblique detonation wave in hypersonic flow," Symp. (Int.) Combust. **27**, 2207 (1998).
[33] M. V. Papalexandris, "A numerical study of wedge-induced detonations," Combust. Flame **120**, 526 (2000).
[34] J. Y. Choi, D. W. Kim, I. S. Jeung, F. Ma, and V. Yang, "Cell-like structure of unstable oblique detonation wave from high-resolution numerical simulation," Proc. Combust. Inst. **31**, 2473 (2007).
[35] M. J. Grismer and J. M. Powers, "Numerical predictions of oblique detonation stability boundaries," Shock Waves **6**, 147 (1996).
[36] J. Verreault, A. J. Higgins, and R. A. Stowe, "Formation of transverse waves in oblique detonations," Proc. Combust. Inst. **34**, 1913 (2013).
[37] H. H. Teng, Z. L. Jiang, and H. D. Ng, "Numerical study on unstable surfaces of oblique detonations," J. Fluid Mech. **744**, 111 (2014).
[38] H. Teng, H. D. Ng, K. Li, C. Luo, and Z. Jiang, "Evolution of cellular structures on oblique detonation surfaces," Combust. Flame **162**, 470 (2015).
[39] P. Yang, H. Teng, H. D. Ng, and Z. Jiang, "A numerical study on the instability of oblique detonation waves with a two-step induction-reaction kinetic model," Proc. Combust. Inst. (to be published).
[40] M. Reynaud, F. Virot, and A. Chinnayya, "A computational study of the interaction of gaseous detonations with a compressible layer," Phys. Fluids **29**, 056101 (2017).
[41] X. C. Mi, A. J. Higgins, C. B. Kiyanda, H. D. Ng, and N. Nikiforakis, "Effect of spatial inhomogeneities on detonation propagation with yielding confinement," Shock Waves **28**, 993–1009 (2018).
[42] C. Li, K. Kailasanath, and E. S. Oran, "Effects of boundary layers on oblique detonation structures," AIAA Paper No. 93-0450, 1993.
[43] I. Mahle, H. Foysi, S. Sarkar, and R. Friedrich, "On the turbulence structure in inert and reacting compressible mixing layers," J. Fluid Mech. **593**, 171–180 (2007).
[44] T. Mai, Y. Sakimitsu, H. Nakamura, Y. Ogami, T. Kudo, and H. Kobayashi, "Effect of the incident shock wave interacting with transversal jet flow on the mixing and combustion," Proc. Combust. Inst. **33**, 2335–2342 (2011).
[45] C. Huete, A. L. Sánchez, F. A. Williams, and J. Urzay, "Diffusion-flame ignition by shockwave impingement on a supersonic mixing layer," J. Fluid Mech. **784**, 74–108 (2015).
[46] C. Huete, A. L. Sánchez, and F. A. Williams, "Diffusion-flame ignition by shock-wave impingement on a hydrogen-air supersonic mixing layer," J. Propul. Power **28**, 256–263 (2016).
[47] P. J. Ferrer, G. Lehnasch, and A. Mura, "Compressibility and heat release effects in highspeed reactive mixing layers II. Structure of the stabilization zone and modeling issues relevant to turbulent combustion in supersonic flows," Combust. Flame **180**, 304–320 (2017).
[48] Z. Ren, B. Wang, and L. X. Zheng, "Numerical analysis on interactions of vortex, shock wave, and exothermal reaction in a supersonic planar shear layer laden with droplets," Phys. Fluids **30**, 036101 (2018).
[49] E. F. Toro, *Riemann Solvers and Numerical Methods for Fluid Dynamics*, 2nd ed. (Springer, Berlin, 1999).
[50] G. J. Sharpe and M. I. Radulescu, "Statistical analysis of cellular detonation dynamics from numerical simulations: One-step chemistry," Combust. Theory Modell. **15**, 691 (2011).